

# Goal-Oriented Learning at the Edge: Graph Neural Networks Over-the-Air for Blockage Prediction

Lorenzo Mario Amorosa, *Member, IEEE*, Zhan Gao, *Graduate Student Member, IEEE*, Tony Chahoud, *Member, IEEE*, Yiqun Wu, Lukas Eller, Marco Skocaj, Roberto Verdone, *Senior Member, IEEE*

**Abstract**—Sixth-generation (6G) wireless networks evolve from connecting devices to connecting intelligence. The focus turns to *Goal-Oriented Communications*, where the effectiveness of communication is assessed through task-level objectives over traditional throughput-centric metrics. As communication intertwines with learning at the edge, distributed inference over wireless networks faces a critical trade-off between task accuracy and efficient radio resource use. Traditional communication schemes (e.g., OFDMA) are not designed for this trade-off, often facing challenges related to scalability and latency. Therefore, we propose a novel goal-oriented framework that integrates over-the-air computation with spatio-temporal graph learning. Leveraging the wireless channel as an analog aggregation layer, the proposed framework enables low-latency message passing while efficiently aggregating semantically relevant features from distributed nodes. Theoretical analysis confirms that our analog architecture converges to the expressive power of digital message passing, while offering decisive scalability advantages. We assess the framework in proactive line-of-sight blockage prediction for millimeter-wave networks. Through high-fidelity ray-tracing simulations, the framework exhibits strong inductive generalization to unseen networks and adapts to domain shifts via lightweight transfer learning, matching or even outperforming digital baselines with significantly reduced communication overhead.

**Index Terms**—Sixth-generation (6G), Goal-Oriented Communication, Over-the-Air Computation (AirComp), Graph Neural Networks (GNN), Industrial IoT (IIoT), Blockage Prediction, mmWave.

## I. INTRODUCTION

THE evolution of wireless networks toward sixth generation (6G) is driving a fundamental paradigm shift from purely connecting devices to connecting intelligence [1, 2]. The rapid proliferation of artificial intelligence (AI)-driven services and applications, combined with the envisioned role of 6G as an enabler of distributed intelligence at the network edge [3] necessitates a change in network design: rather than simply optimizing for bit-rates or packet error rates, the focus turns to the effect of communication in the expected improvement of a task-specific objective [4]. This necessitates *Goal-Oriented Communications* [5], where the design of communications schemes becomes an integral component of learning algorithms at the edge, and joint optimization of communication

and learning aims to fulfill specific downstream tasks, such as control, anomaly detection, or sensing, rather than merely targeting generic quality-of-service (QoS) metrics [6].

However, effective deployments of distributed inference over wireless networks, especially in industrial Internet-of-things (IIoT) settings, face a critical trade-off between task accuracy and efficient radio resource use. On one hand, robust decision-making typically requires cooperation among nodes to fuse information from multiple spatially distributed nodes [7, 8]. On the other hand, the resulting predictions must be produced within strict deadlines to enable timely control actions and avoid system failures [9]. Standard communication systems are designed to maximize the reliable delivery of individual data streams, employing orthogonal resource allocation (e.g., time division multiple access (TDMA), orthogonal frequency division multiple access (OFDMA)) to isolate users and eliminate interference. While robust, this creates a scalability barrier: in dense industrial networks, the finite availability of radio resources limits the number of devices that can coordinate for a cooperative task through simultaneous transmissions. As a result, the latency incurred to collect reliable data from all relevant sensors often exceeds application requirements, making the inference obsolete [10].

To overcome these limitations, *over-the-air computation* (*AirComp*) has emerged as a transformative physical-layer technique [11]. By integrating computation directly into the transmission phase, AirComp allows concurrent transmissions to exploit the superposition property of the wireless channel to aggregate signals from multiple nodes over-the-air, enabling all sensors to transmit simultaneously on the same time-frequency resources without decoding individual streams [12]. This analog aggregation paradigm is particularly synergistic with graph neural networks (GNNs), where the dominant operation is the aggregation of feature vectors from neighboring nodes [13–15]. This has given rise to *over-the-air graph neural networks* (*AirGNNs*) [16], architectures that map the graph topology onto the wireless network, utilizing the channel as an intrinsic processing layer of the neural model. These architectures jointly optimize communication and learning at the edge by leveraging AirComp for the simultaneous transmission of neighboring nodes, effectively performing feature aggregation in the analog domain. This grants the system lower communication latency and higher spectral efficiency over traditional orthogonal multiple access schemes, while preserving the accuracy of graph-based learning tasks and enabling scalable distributed inference across edge devices.

In this paper, we investigate this goal-oriented paradigm through the lens of a critical IIoT use case: *LOS blockage prediction* for millimeter-wave (mmWave) networks. High-frequency wireless links are essential for next-generation industrial automation [17, 18]. The large bandwidth available

L.M. Amorosa and R. Verdone are with the Department of Electrical, Electronic and Information Engineering (DEI), “Guglielmo Marconi”, University of Bologna & WiLab - National Wireless Communication Laboratory (CNIT), Bologna, Italy. E-mail: {lorenzomario.amorosa, roberto.verdone}@unibo.it

Z. Gao is with the Department of Computer Science and Technology, University of Cambridge, Cambridge, U.K. E-mail: zg292@cam.ac.uk

T. Chahoud is with WiLab - National Wireless Communication Laboratory (CNIT), Bologna, Italy. E-mail: tony.chahoud@wilab.cnit.it

Y. Wu is with Huawei Technologies Co., Ltd., RAN Research Department, Shanghai, China. E-mail: wuyiqun@huawei.com

L. Eller and M. Skocaj are with Huawei Heisenberg Research Center (Munich), Germany. E-mail: {lukas.eller,marco.skocaj}@huawei.com

Corresponding author: Zhan Gao.

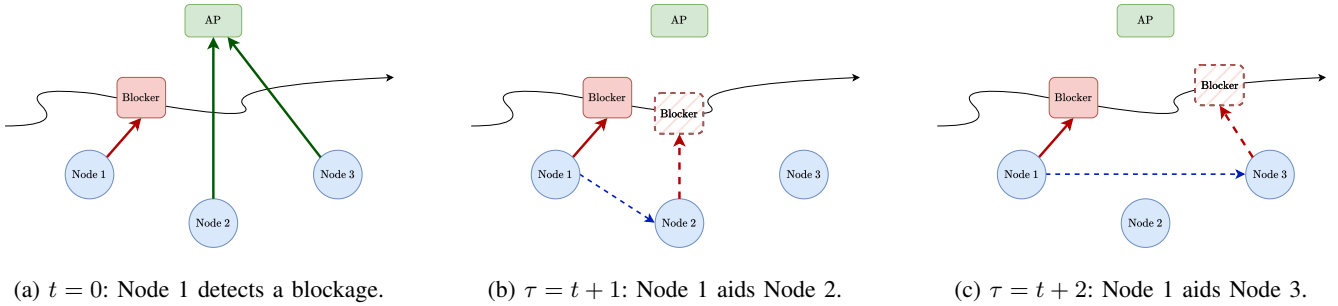


Fig. 1: Example scenario illustrating the dependence of node cooperation on the prediction horizon  $\tau$ . (a) At  $t = 0$ , Node 1 detects a mobile blocker while Nodes 2 and 3 maintain line-of-sight (LOS). (b) For a short prediction horizon ( $\tau = t + 1$ ), Node 2 is informed by Node 1 to predict the incoming blocker. (c) For a longer horizon ( $\tau = t + 2$ ), the relevance of information shifts; Node 3 must now cooperate with Node 1 to anticipate the blocker's arrival.

at these frequencies supports novel use cases, such as high-resolution wireless sensing, real-time control of mobile robots, and ultra-reliable links for automation [19, 20]. However, despite offering wide spectral resources, these frequencies suffer significant molecular absorption, scattering, and blockages, which together frequently cause severe link degradation and abrupt outages [21, 22]. Proactive blockage prediction is, therefore, a strict requirement for reliability [23]. This problem serves as an ideal case study for goal-oriented communications for two reasons. First, it requires ultra-low latency inference that digital schemes struggle to support in dense settings. Second, changing the learning objective (e.g., the prediction horizon) directly affects the level of cooperation required among nodes to fuse information, as illustrated in Fig. 1, thereby necessitating the joint optimization of communication strategies and learning parameters. By allowing the channel to participate in distributed decision-making via AirComp, we do not just aim at efficient radio resource use; instead, we leverage the physics of propagation to solve the prediction task [24]. To this end, we propose *goal-oriented spatio-temporal over-the-air graph neural networks (GO-ST-AirGNNs)*, a goal-oriented communication framework based on frequency-selective spatio-temporal AirGNNs. Our specific contributions are summarized as follows:

- 1) We propose GO-ST-AirGNN, a unified framework that integrates over-the-air computation with spatio-temporal graph learning. By treating the wireless channel as an analog processing layer, the framework enables scalable, spectral-efficient feature aggregation in dense distributed networks.
- 2) We develop a goal-oriented radio resource management (RRM) scheme that acts as a physical attention mechanism. Unlike conventional approaches that maximize throughput, our method optimizes transmission power and spectral resources to minimize downstream prediction error, prioritizing semantically relevant features.
- 3) We provide theoretical analysis for the spectral efficiency and expressive power of the proposed architecture. We demonstrate that GO-ST-AirGNN achieves spectral-efficient scalability independent of node density by utilizing a constant number of radio resources for feature aggregation. Furthermore, we prove that with sufficient spectral resources the proposed architecture gains the universal approximation capability to emulate

standard message passing neural networks (MPNNs).

- 4) We validate the framework using high-fidelity ray-tracing simulations in IIoT environments. Results demonstrate that GO-ST-AirGNN generalizes effectively to unseen scenarios and domain shifts, matching digital baselines while significantly reducing communication overhead.

The remainder of the paper is organized as follows. Section II reviews related works. Section III formalizes the system model and the problem formulation. Section IV presents the GO-ST-AirGNN architecture. Section V formalizes the spectral efficiency and expressive power of GO-ST-AirGNN. Section VI discusses the learning procedure and deployment of the proposed architecture. Section VII reports the numerical results. Section VIII concludes the manuscript.

## II. RELATED WORK

Running inference tasks at the edge in next-generation IIoT networks requires accurate short-term forecasting of the wireless environment, including proactive blockage prediction [25]. Data-driven approaches are emerging for modeling non-linear channel dynamics, often treating the channel as a time-series where historical features reveal latent blocker trajectories [26]. In this context, *wireless signatures* derived from standard power measurements allow the network to predict blockage events without dedicated hardware [27]. However, purely radio frequency (RF)-based methods often lack explicit geometric awareness, necessitating the use of multimodal fusion. While LiDAR-based fusion offers superior spatial precision [28] and RGB-based methods effectively calculate interception probabilities [29], they face cost, privacy, and low-light limitations. Alternatively, radar sensors provide a privacy-preserving option, utilizing range-velocity maps for precise blockage timing [30].

Crucially, single-link models fail to capture network-wide spatial correlations. To address this, spatio-temporal graph neural networks (ST-GNNs) have been adopted to model blockage dependencies by aggregating neighbor information via message passing [31]. This spatial efficacy is further validated in power management [32], handover forecasting [33], and dynamic cell-free multiple-input multiple-output (MIMO) coverage prediction [34], as systematically reviewed in [35]. However, standard digital GNN implementations relying on orthogonal multiple access suffer from poor scalability, as

resource requirements scale linearly with neighborhood size [36]. In contrast, AirComp mitigates this by exploiting channel superposition for analog aggregation, decoupling bandwidth consumption from the number of neighbors [37].

AirComp has been extensively studied for federated learning (FL), where the goal is to aggregate local gradients over the air [38]. To ensure that signals add up constructively, channel phases must be synchronized. Authors in [39] introduce reconfigurable intelligent surfaces (RIS) to shape the channel environment for AirComp. The integration of GNN with AirComp exploits a natural synergy, as the neighbor aggregation in GNN message passing maps directly to the signal superposition property of the wireless channel. The work in [16] rigorously analyzes the stability of GNNs when the aggregation is performed over a noisy, fading channel. Instead of training a GNN on ideal data and deploying it on a noisy channel (which leads to degradation), authors incorporate the channel's fading and noise statistics into the training loop, learning neural network weights that are inherently robust to channel impairments. The paper in [40] proposes a "channel-inversion" transmission strategy: if the physical channel does not match the desired graph topology, nodes can use precoding to transmit their signals such that the effective channel approximates the graph signal, allowing the execution of arbitrary graph convolutions over physical wireless links. Beyond spectral efficiency, AirGNNs offer privacy advantages. Because individual neighbor features are summed in the air before reaching the receiver, the receiver cannot isolate the raw data of any single neighbor, which provides intrinsic physical-layer privacy for sensitive sensor data [41].

Goal-oriented and semantic communication have emerged as key enablers for modern control systems and wireless network [42, 43]. To realize this approach, authors in [44] propose a deep reinforcement learning (DRL)-driven agent that learns to allocate resource blocks based on the semantic importance of the data. Crucially, the reward function here is tied explicitly to task performance metrics rather than conventional data rates. Goal-oriented communication often integrates concepts like the value of information (VoI) alongside age of information (AoI). As demonstrated in [45], minimizing AoI is not always optimal; an older packet with high semantic density (e.g., a critical keyframe) may yield a higher reward than fresher, redundant updates. Finally, this focus on utility naturally leads to semantic compression, where the objective shifts from transmitting data efficiently to transmitting less data overall [46].

Despite these advances, a unified framework integrating the spatial awareness of ST-GNNs, the scalability of AirComp, and goal-oriented utility is missing. Existing AirGNN frameworks typically treat wireless transmission and graph inference as distinct optimization stages, limiting efficacy in dynamic blockage prediction. To address this, we propose GO-ST-AirGNN, a framework that jointly optimizes RRM and learning parameters, ensuring resource allocation is driven explicitly by the semantic value of the prediction task.

### III. LOS BLOCKAGE PREDICTION PROBLEM

#### A. System Model

We consider a wireless IIoT network comprising a set of full-duplex single-antenna wireless nodes  $\mathcal{N} = \{1, \dots, N\}$  served by a central controller or AP. The nodes operate

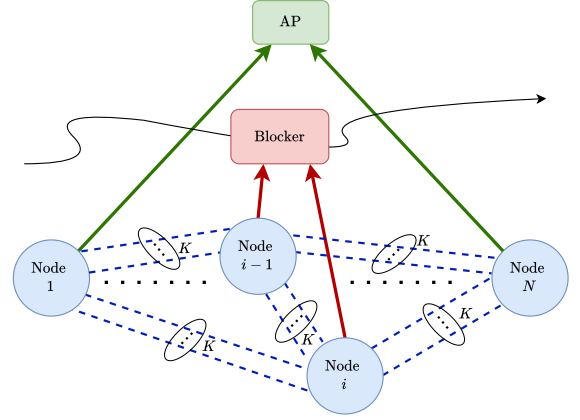


Fig. 2: The network contains a set of wireless nodes  $\mathcal{N}$  served by a central access point (AP). The direct links are susceptible to blockage by dynamic obstacles, leading to non-line-of-sight (NLOS) conditions. To anticipate these events, nodes cooperate by exchanging local features  $\mathbf{x}_{i,t}$  over  $K$  parallel dynamic communication graphs  $\{\mathcal{G}_{t,k}\}_{k=1}^K$ , leveraging AirComp to aggregate information, and predicting the future blockage status  $y_{i,t+\tau}$ .

in the mmWave frequency band and necessitate strict LOS connectivity to the AP. We consider a dynamic system where time is slotted into discrete intervals  $t \in \{1, \dots, T\}$ . At any time slot  $t$ , the propagation environment may vary due to the movement of mobile obstacles within the industrial area. These obstacles can temporarily shadow the communication links, causing NLOS blockage events. The critical link requiring monitoring is the direct channel between node  $i \in \mathcal{N}$  and the AP, denoted by  $\mathbf{h}_{i,t}^{\text{AP}} \in \mathbb{C}$ . To anticipate the reliability of this link, we define a binary blockage label  $y_{i,t+\tau} \in \{0, 1\}$  with a future prediction horizon  $\tau$ . Here,  $y_{i,t+\tau} = 1$  indicates a blockage (NLOS) event, while  $y_{i,t+\tau} = 0$  denotes a clear LOS condition.

Since nodes do not possess global knowledge of the environment, they rely on local channel estimations to infer future states. At each time slot  $t$ , each node  $i$  constructs a feature vector  $\mathbf{x}_{i,t} \in \mathbb{R}^L$  encapsulating the local temporal evolution of the wireless channel. For instance,  $\mathbf{x}_{i,t}$  may consist of a sliding window of historical channel gains as

$$\mathbf{x}_{i,t} = [|\mathbf{h}_{i,t}^{\text{AP}}|, |\mathbf{h}_{i,t-1}^{\text{AP}}|, \dots, |\mathbf{h}_{i,t-L+1}^{\text{AP}}|]^{\top}. \quad (1)$$

To cooperate and improve prediction accuracy, nodes can exchange their local features  $\mathbf{x}_{i,t}$  at time slot  $t$  over  $K$  orthogonal frequency resources (or subcarriers), modeled as  $K$  parallel dynamic communication graphs  $\{\mathcal{G}_{t,k}\}_{k=1}^K$ . The existence of edges in these graphs is determined by the wireless channel conditions and the resource allocation strategy. Specifically, at each time  $t$ , let  $\mathbf{h}_{i,j,k,t} \in \mathbb{C}$  be the channel coefficient between node  $i$  and node  $j$  on frequency  $k$ . Every node  $i$  allocates a transmit power vector  $\mathbf{p}_{i,t} = [p_{i,1,t}, \dots, p_{i,K,t}]^{\top} \in \mathbb{R}_+^K$  across the  $K$  subcarriers, and the edge set for the  $k$ -th frequency is defined as

$$\mathcal{E}_{t,k} = \left\{ (i, j) \in \mathcal{N}^2 : i \neq j, \frac{p_{i,k,t} \mathbb{E}[|\mathbf{h}_{i,j,k,t}|^2]}{\sigma^2} \geq \gamma_{\min} \right\}. \quad (2)$$

where the channel expectation  $\mathbb{E}[|\mathbf{h}_{i,j,k,t}|^2]$  is computed over small scale fading,  $\sigma^2$  is the thermal noise at the receiver, and  $\gamma_{\min}$  is the receiver sensitivity. Consequently, the topology of the  $k$ -th graph  $\mathcal{G}_{t,k}$  is dynamic and frequency-selective; an edge  $(i, j)$  exists only if condition (2) is satisfied. An overview of the scenario is provided in Fig. 2.

### B. Problem Formulation

The primary objective of the network is to predict the future blockage status of all nodes. We formulate this as a supervised learning task where the predicted status  $\hat{y}_{i,t+\tau}$  is the output of a function  $f_i(\cdot; \boldsymbol{\theta})$  parameterized by  $\boldsymbol{\theta}$ . The prediction function relies on the feature states of the nodes  $\mathbf{X}_t = [\mathbf{x}_{1,t}, \dots, \mathbf{x}_{N,t}]$  and the communication graphs shaped by the power allocation  $\mathbf{p}_t = [\mathbf{p}_{1,t}, \dots, \mathbf{p}_{N,t}]$  [cf. (2)] as

$$\hat{y}_{i,t+\tau} = f_i\left(\mathbf{X}_t, \{\mathcal{G}_{t,k}(\mathbf{p}_t)\}_{k=1}^K; \boldsymbol{\theta}\right). \quad (3)$$

To measure the prediction quality, we utilize the binary cross-entropy (BCE) loss function. The network-wide loss at time  $t$  is defined as:

$$\mathcal{J}_t(\boldsymbol{\theta}, \mathbf{p}_t) = -\frac{1}{N} \sum_{i=1}^N \mathbb{E} \left[ y_{i,t+\tau} \log(\hat{y}_{i,t+\tau}) + (1 - y_{i,t+\tau}) \log(1 - \hat{y}_{i,t+\tau}) \right]. \quad (4)$$

We aim to jointly optimize the prediction model parameters  $\boldsymbol{\theta}$  and the goal-oriented power allocation  $\mathbf{p}_t$ . Unlike standard RRM which maximizes data rates, our goal-oriented framework designs the power allocation strategy to shape the topology of communication graphs  $\mathcal{G}_{t,k}(\mathbf{p}_t)$  and support the prediction model to minimize the prediction error. Given a total power budget  $P_{\text{tot}}$  at each node, the joint optimization problem is formulated as:

$$\min_{\boldsymbol{\theta}, \mathbf{p}_t} \mathcal{J}_t(\boldsymbol{\theta}, \mathbf{p}_t) \quad (5a)$$

$$\text{s.t.} \quad \sum_{k=1}^K p_{i,k,t} \leq P_{\text{tot}}, \quad \forall i \in \mathcal{N}, \quad (5b)$$

$$p_{i,k,t} \geq 0, \quad \forall i \in \mathcal{N}, \forall k \in \{1, \dots, K\}. \quad (5c)$$

This formulation encourages a goal-oriented communication strategy: by allocating transmit power to specific subcarriers, nodes effectively establish edges in the dynamic graphs  $\{\mathcal{G}_{t,k}\}_{k=1}^K$ , enabling the flow of features  $\mathbf{x}_{i,t}$  required for cooperative sensing.

## IV. GOAL-ORIENTED ARCHITECTURE

To address the joint problem of resource allocation and blockage prediction, we propose GO-ST-AirGNN, a unified goal-oriented framework that couples over-the-air computation with spatio-temporal graph learning. Unlike conventional GNNs that assume perfect digital exchanges of node features followed by local processing, the proposed architecture integrates the communication channel directly into the learning loop, treating the physical medium as an inherent processing layer. This design leverages the waveform superposition property of the wireless channel to perform spectral-efficient feature aggregation via AirComp. Moreover, it accounts for

both spatial and temporal information for resource allocation and blockage prediction, which addresses the joint problem in a comprehensive manner. Specifically, the GO-ST-AirGNN framework is built upon three fundamental pillars:

- *Over-the-air graph aggregation.* Instead of digitizing, packetizing, and scheduling feature vectors, nodes transmit analog signals simultaneously. GO-ST-AirGNN leverages the superposition property of the wireless channel to naturally compute convolutions over graphs fundamental to GNNs.
- *Goal-oriented communications.* By optimizing the resource allocation vector  $\mathbf{p}_t$ , GO-ST-AirGNN dynamically weighs the edges of the communication graph and optimizes the topology to support the blockage prediction model and minimize the prediction loss. This goal-oriented RRM introduces a physical graph attention mechanism. Different from classical graph attention that is typically computed at the receiver, it applies attention directly at the transmitter.
- *Spatio-temporal reasoning.* Blockage events in industrial environments are rarely isolated (e.g., they result from continuously moving obstacles). In this context, GO-ST-AirGNN processes temporal sequences of local features  $\mathbf{X}_t$  over the graph temporal process  $\{\mathcal{G}_{t,k}\}$  to capture the spatio-temporal correlations necessary for future blockage prediction.

The architecture decomposes the blockage prediction task into three stages: (i) a *semantic encoder*, which determines the transmission policy of local features, (ii) an *over-the-air aggregation layer*, which conducts the feature aggregation with AirComp, and (iii) a *semantic decoder*, which performs the downstream blockage prediction. The overall architecture is depicted in Fig. 3.

### A. Semantic Encoder and Transmission Policy

In the proposed GO-ST-AirGNN architecture, the transmission stage at each node  $i$  is decoupled into two parallel learnable processes: *semantic embedding* and *resource management*. The former learns higher-level representations from local features to determine transmission content, while the latter learns the frequency-aware power allocation strategy to determine transmission policy. At time slot  $t$ , node  $i$  processes its local feature vector  $\mathbf{x}_{i,t}$  through two neural networks:

1) *Message Embedding:* First, a semantic encoder  $\Phi_i(\cdot)$ , parameterized by weights  $\boldsymbol{\theta}_{i,\Phi}$ , maps the input features to a normalized message embedding vector

$$\mathbf{m}_{i,t} = \frac{\Phi_i(\mathbf{x}_{i,t}; \boldsymbol{\theta}_{i,\Phi})}{|\Phi_i(\mathbf{x}_{i,t}; \boldsymbol{\theta}_{i,\Phi})|^2}. \quad (6)$$

This vector represents the semantic content to be communicated across the  $K$  subcarriers. The normalization ensures that  $\mathbf{m}_{i,t}$  has unit power prior to being scaled by the transmit power allocation, specified in the subsequent section.

2) *Resource Management:* Second, a resource management module  $\Psi_i(\cdot)$ , parameterized by weights  $\boldsymbol{\theta}_{i,\Psi}$ , maps the input features to a power allocation vector

$$\mathbf{p}_{i,t} = \Psi_i(\mathbf{x}_{i,t}; \boldsymbol{\theta}_{i,\Psi}). \quad (7)$$

This vector determines the transmission amplitude for each subcarrier. The output of  $\Psi_i$  is constrained to be non-negative and to satisfy (5b) and (5c) through a softmax-based activation function at the output layer.

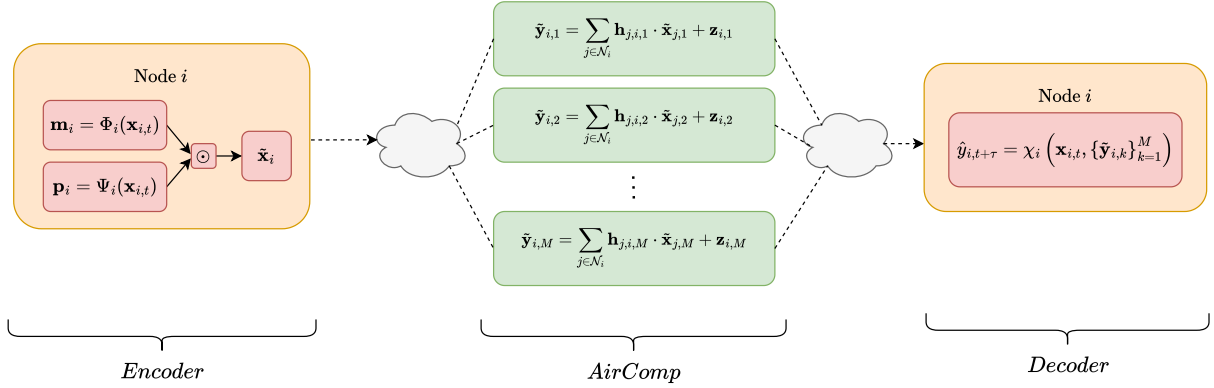


Fig. 3: Overview of the proposed GO-ST-AirGNN architecture. (Left) At the transmitter, node  $i$  uses a semantic encoder  $\Phi_i$  and a resource manager  $\Psi_i$  to jointly generate the message embedding  $\mathbf{m}_i$  and the goal-oriented power allocation vector  $\mathbf{p}_i$ . (Center) The wireless channel acts as a computation layer (AirComp), naturally aggregating neighbor signals via electromagnetic superposition across the parallel dynamic communication graphs. (Right) At the receiver, the semantic decoder  $\chi_i$  processes the aggregated analog signals  $\tilde{\mathbf{y}}_{i,k}$  together with the local features to predict the future blockage status  $\hat{y}_{i,t+\tau}$ .

3) *Goal-Oriented Transmission*: Finally, the transmitted signal  $\tilde{\mathbf{x}}_{i,t}$  is obtained via Hadamard product of the power allocation vector and the message embedding, i.e.,

$$\tilde{\mathbf{x}}_{i,t} = \mathbf{p}_{i,t} \odot \mathbf{m}_{i,t}. \quad (8)$$

In this context, the semantic encoder not only learns the transmitted content but also learns the transmission power; together, yielding a goal-oriented communication strategy. By optimizing  $\theta_{i,\Phi}$  and  $\theta_{i,\Psi}$  w.r.t. the final prediction loss, the node weighs message embeddings with physical attention by allocating power to subcarriers and formulates communication graphs to emphasize features that carry the most relevant information regarding the blockage event.

### B. Over-the-Air Aggregation Layer

The core component of GO-ST-AirGNN is the use of the wireless channel as a computational layer to perform graph convolutions with over-the-air computation (AirComp). Specifically, it employs an AirComp scheme to aggregate the generated message embeddings [Section IV-A] from neighbors via uncoded analog communication [37]. Unlike digital schemes that transmit data packets orthogonally, AirComp leverages the superposition property of the wireless channel to perform data aggregation directly in the analog domain. This grants superior spectral efficiency and ultra-low latency, enabling the required communication resources to remain constant regardless of the number of transmitting neighbors.

Each node  $i$  transmits  $\tilde{\mathbf{x}}_{i,t}$  across the  $K$  available frequency subcarriers. We denote by  $\tilde{\mathbf{x}}_{i,k,t}$  the analog signal transmitted by node  $i$  on subcarrier  $k$ . The signal received at a generic node  $j$  is the electromagnetic superposition of transmitted signals from its neighbors. It is important to note that aggregation of neighboring signals occurs spatially but is maintained orthogonally across frequencies<sup>1</sup>. Consequently, the total bandwidth is utilized such that the signals transmitted

on different subcarriers remain spectrally distinct. Specifically, the signal received at node  $i$  on frequency  $k$  is given by:

$$\tilde{\mathbf{y}}_{i,k,t} = \sum_{j \in \mathcal{N}_i} \mathbf{h}_{j,i,k,t} \tilde{\mathbf{x}}_{j,k,t} + \mathbf{z}_{i,k,t}, \quad (9)$$

where  $\mathbf{z}_{i,k,t} \sim \mathcal{CN}(0, \sigma^2)$  represents the additive white Gaussian noise and  $\sigma^2$  is the noise variance. The node  $i$  then collects the vector of received signals  $\tilde{\mathbf{y}}_{i,t} = [\tilde{\mathbf{y}}_{i,1,t}, \dots, \tilde{\mathbf{y}}_{i,K,t}]$  over the  $K$  subcarriers. This is a  $K$ -dimensional aggregated message, where each dimension corresponds to a specific communication graph  $\mathcal{G}_{t,k}$  and the graph topology is determined by the allocated power.

### C. Semantic Decoder and LOS Blockage Prediction

The final stage of the GO-ST-AirGNN pipeline takes place at the receiver side of node  $i$ . Here, the physical analog signals  $\tilde{\mathbf{y}}_{i,t}$  received over-the-air are processed to predict future LOS blockages. To recover the specific blockage probability, node  $i$  employs a semantic decoder function  $\chi_i(\cdot)$ , parameterized by weights  $\theta_{i,\chi}$ . This module acts as the readout head of the GNN. Since blockage events are dynamic processes, the decoder must reason over time. Therefore, we define the input to the decoder not just as the instantaneous reception, but as a history of both local features and spatially aggregated context. Specifically, we denote by  $\mathbf{s}_{i,t}$  the combined state at time  $t$ :

$$\mathbf{s}_{i,t} = [\mathbf{x}_{i,t} \parallel \mathbf{y}_{i,t}], \quad (10)$$

where  $\parallel$  denotes concatenation. The semantic decoder  $\chi_i$  processes a sliding window of these states to capture temporal dependencies. The estimated blockage probability  $\hat{y}_{i,t+\tau}$  is given by:

$$\hat{y}_{i,t+\tau} = \chi_i \left( \{\mathbf{s}_{i,t'}\}_{t'=t-L+1}^t; \theta_{i,\chi} \right). \quad (11)$$

Functionally,  $\chi_i$  can be implemented as a sequence-based model (e.g., recurrent neural networks (RNNs) or a temporal convolutional layer) followed by a binary classification head. We can then make predictions based on  $\hat{y}_{i,t+\tau}$ .

<sup>1</sup>To operate the  $K$  parallel dynamic graphs, the total bandwidth  $B$  is divided into  $K$  uniformly spaced subcarriers. To strictly avoid inter-carrier interference, each subcarrier  $k$  is allocated a bandwidth of  $B_k = \frac{B - \Delta f}{K}$ , separated by a guard-band  $\Delta f$ .

## V. THEORETICAL ANALYSIS

### A. Spectral Efficiency

A critical challenge in dense IIoT deployments is maintaining spectral-efficient operations as the network density increases. In this section, we formalize the advantage of GO-ST-AirGNN in terms of communication scalability, compared to standard digital baselines. We consider a network modeled by a graph  $\mathcal{G} = (\mathcal{N}, \mathcal{E})$ , where each node  $i \in \mathcal{N}$  must aggregate features from its neighborhood  $\mathcal{D}_i$  over  $K$  orthogonal resource blocks. We define the *communication cost*  $T_{\text{air}}$  and  $T_{\text{dig}}$  as the number of time slots required for all nodes in  $\mathcal{N}$  to complete a graph convolution (aggregation) step across the network for analog and digital approaches, respectively.

**Proposition 1 ( $O(1)$  Communication Cost in GO-ST-AirGNN).** Let  $\Delta(\mathcal{G}) = \max_{i \in \mathcal{N}} |\mathcal{D}_i|$  denote the maximum node degree, which represents the size of the largest neighborhood in  $\mathcal{G}$ , and, therefore, the number of messages that the node with most neighbors receives during an aggregation step. The communication cost for GO-ST-AirGNN ( $T_{\text{air}}$ ) and the lower bound for a digital baseline ( $T_{\text{dig}}$ ) scale as follows:

$$T_{\text{air}} = 1, \quad T_{\text{dig}} \geq \left\lceil \frac{\Delta(\mathcal{G})}{K} \right\rceil, \quad (12)$$

where  $\lceil \cdot \rceil$  is the ceil operator.

*Proof.* See the Appendix.

Proposition 1 states that the asymptotic communication complexity of GO-ST-AirGNN is  $O(1)$ , whereas that of the digital scheme is  $O(\Delta(\mathcal{G}))$ . Crucially, the former is independent of the graph connectivity, while the latter is degree-limited. This result establishes a critical scalability advantage of our framework. As the network gets denser, the proposed GO-ST-AirGNN maintains constant communication cost  $T_{\text{air}}$ , independently of the local node density. In contrast, the spectral-efficiency of digital approaches degrades, creating a bottleneck for real-time inference.

### B. Expressive Power

While the primary advantage of GO-ST-AirGNN lies in its spectral efficiency and low-latency analog aggregation via AirComp, it is theoretically significant to establish its representational capacity compared to standard digital GNNs. Typically, GNNs rely on the MPNN framework, where nodes exchange discrete feature vectors to compute updates. A concern with analog aggregation may be that the physical channel forces a specific aggregation operator (i.e., summation) and restricts the degrees of freedom to model graph structures, as the aggregation is bound by channel conditions and RRM rather than allowing for the full signal separation typical of digital MPNNs. In this section, we formally analyze the expressive power of the proposed architecture at a fixed time slot  $t$ . We demonstrate that with sufficient resource units, i.e., if the number of subcarriers  $K$  is sufficiently large to ensure every neighbor  $j$  of a target node  $i$  transmits on a unique, interference-free frequency, GO-ST-AirGNN can decode individual messages. Consequently, it satisfies the prerequisites to emulate standard MPNN neighborhood aggregation and is capable of approximating any standard MPNN layer at any time slot  $t$ . Specifically, in a generic update layer of a standard

MPNN, for a node  $i$  with hidden state  $\mathbf{u}_i \in \mathbb{R}^d$ , the updated state  $\mathbf{u}'_i$  is computed as

$$\mathbf{u}'_i = \mathcal{U} \left( \mathbf{u}_i, \bigoplus_{j \in \mathcal{N}_i} \mathcal{M}(\mathbf{u}_i, \mathbf{u}_j) \right), \quad (13)$$

where  $\mathcal{M}(\cdot)$  is a learnable message function,  $\bigoplus$  is a permutation-invariant aggregation operator (e.g., sum, mean, or max), and  $\mathcal{U}(\cdot)$  is a state update function. In this digital abstraction, messages are transmitted reliably and orthogonally. We now show that the proposed analog architecture subsumes the generic MPNN formulation under specific conditions.

**Proposition 2 (Universal Approximation via GO-ST-AirGNN).** If the number of subcarriers is  $K = K'$ , where  $K'$  is the number of subcarriers required to ensure that for every node  $i$ , all incoming signals from its neighbors  $j \in \mathcal{N}_i$  are mapped to mutually orthogonal frequencies, and assuming a high-signal-to-noise ratio (SNR) regime (i.e.,  $\frac{P_{\text{tot}}}{\sigma^2} \rightarrow \infty$ ), the GO-ST-AirGNN architecture can approximate the generic MPNN update rule defined in (13) with arbitrary precision at any given time slot  $t$ .

*Proof.* See the Appendix.

Proposition 2 establishes that the analog nature of GO-ST-AirGNN does not inherently limit its reasoning capabilities compared to digital counterparts. It proves that, with sufficient bandwidth, the system gains the degrees of freedom to emulate any arbitrary message passing logic via over-the-air aggregation. It is interesting to see that the number of subcarriers  $K$  regulates the trade-off between expressivity and latency. Approaching  $K \approx K'$  recovers the full separation capabilities of digital MPNNs at the cost of bandwidth, whereas a smaller  $K$  fully exploits AirComp to maximize spectral efficiency at the expense of signal resolution. Moreover, in moderate SNR regimes, the stochasticity due to thermal noise during the over-the-air aggregation step can act as a regularization term and improve robustness against overfitting.

## VI. LEARNING PROCEDURE AND DEPLOYMENT

The proposed GO-ST-AirGNN integrates communication and computation into a single differentiable pipeline. This structure allows us to adopt a centralized-training decentralized-execution (CTDE) paradigm [47–49]. While the analog aggregation over physical channels is employed in both training and execution, the training phase leverages centralized parameter sharing to jointly optimize transmission and prediction rules. In the deployment phase, nodes decouple from this central coordination to execute the learned policies in a fully distributed manner using only local information.

### A. End-to-End Optimization

The training objective is to find the optimal set of parameters  $\Theta = \{\theta_{i,\Phi}, \theta_{i,\Psi}, \theta_{i,\chi}\}_{i=1}^N$  that minimizes the long-term blockage prediction loss. Since the wireless channel operations in AirComp are linear and differentiable, the entire system from the semantic encoder at the transmitter to the semantic decoder at the receiver can be modeled as a single computational graph. We consider a training dataset  $\mathcal{T}$  consisting of sequences of channel realizations, node features, and ground-truth blockage labels. The optimization problem is to minimize the expected loss over this dataset:

$$\min_{\Theta} \mathbb{E}_{\mathcal{T}} [\mathcal{J}(\Theta)]. \quad (14)$$

To solve this, we employ a stochastic gradient descent approach. As training is centralized, this error signal propagates from the receiver, through the channel layer, and back to the transmitters, allowing the semantic encoders and decoders to jointly adapt to the wireless environment.

*Remark on the CTDE Paradigm.* The proposed CTDE framework assumes that parameter optimization is performed jointly at a central location, requiring model parameters exchanges over the network. Consequently, we envision the training phase occurring *offline* within a high-fidelity digital twin environment. For future work, we consider extending the framework to a *distributed training-distributed execution* setting.

### B. Decentralized Execution

Once the training converges, the optimized parameter sets  $\{\theta_{i,\Phi}, \theta_{i,\Psi}, \theta_{i,\chi}\}_{i=1}^N$  are deployed to the respective nodes. During the online inference stage, the system operates without any central coordination or global channel knowledge. The execution at each node  $i$  is strictly local:

- 1) *Local sensing.* Node  $i$  collects its local features  $\mathbf{x}_{i,t}$  [cf. (1)].
- 2) *Goal-oriented transmission.* With its trained local models  $\Phi_i$  and  $\Psi_i$ , node  $i$  computes the transmitted content  $\mathbf{m}_{i,t}$  and the transmission power  $\mathbf{p}_{i,t}$  based on  $\mathbf{x}_{i,t}$ , and transmits the analog signal  $\tilde{\mathbf{x}}_{i,t}$  [cf. (8)].
- 3) *Over-the-air aggregation.* Node  $i$  aggregates its neighbors' signals through physical channels via AirComp [cf. (9)].
- 4) *Local blockage prediction.* Node  $i$  concatenates the combined state  $\mathbf{s}_{i,t}$  [cf. (10)], and processes it via  $\chi_i$  to compute the local blockage probability and make the prediction [cf. (11)].

This decentralized architecture ensures that the computational complexity at each node remains constant regardless of the network size, enabling scalable, real-time inference.

*Remark on Synchronization.* Coherent AirComp requires strict phase and time synchronization among transmitting nodes to ensure constructive signal superposition [37]. To this end, many approaches have been investigated. Standard techniques such as timing advance (TA) in 4G Long Term Evolution can facilitate synchronization [50] or reference signal broadcasting can be employed to align transmission windows [51]. Moreover, recent literature addresses synchronization challenges by either exploiting signal approximations to bypass precise timing [52], or by adopting hierarchical architectures with multi-phase relaying [53]. Finally, the propagation characteristics of mmWave frequencies inherently induce highly sparse graph topologies  $\mathcal{G}_{t,k}$ . Unlike sub-6 GHz networks, the strict directionality and blockage of high-frequency links isolate interactions to small subsets of neighbors. This spatial sparsity effectively relaxes the synchronization requirement from a global constraint to a feasible set of local pairwise alignments [54].

## VII. NUMERICAL RESULTS

In this section, we evaluate the performance of the proposed GO-ST-AirGNN framework using a high-fidelity digital twin of the BI-REX Competence Center<sup>2</sup>, simulated via NVIDIA



Fig. 4: Digital twin of the BI-REX Competence Center simulated in NVIDIA Sionna RT. The network consists of distributed IIoT nodes (green spheres) served by a central AP (red sphere). A mobile robot acts as a dynamic blocker, traversing the factory floor and temporarily obstructing the direct LOS communication links between devices and AP.

Sionna RT [55]. The visual representation of the simulation environment is provided in Fig. 4.

### A. Experimental Setup

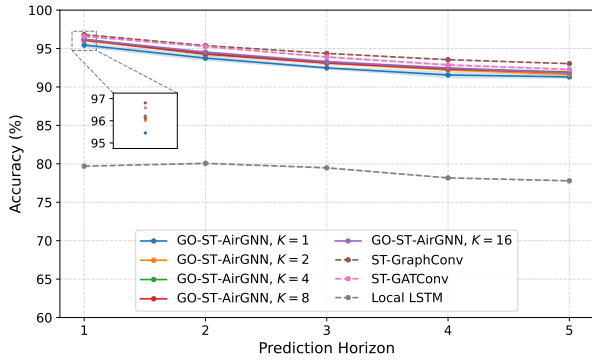
1) *Simulation Environment and Mobility:* The physical propagation environment is modeled as an indoor industrial factory floor (approx. 300 m<sup>2</sup>) populated with static metallic machinery and dynamic obstacles. The primary source of channel variability and blockage is an autonomous mobile robot (AMR) moving through the factory. The AMR follows randomized trajectories with a typical speed of 1 m/s. We discretize time into steps of  $\Delta t \approx 300$  ms. Each simulation sequence consists of  $T = 50$  time steps, corresponding to approximately 15 m of robot travel path per episode. This high temporal resolution captures the gradual onset and resolution of shadowing events caused by the moving blocker.

2) *Network Configuration and Frequency Planning:* The network consists of a set of static IIoT nodes (green nodes in Fig. 4) communicating with a central AP (red node). The communication operates in the mmWave band, centered at  $f_c = 28$  GHz. To enable the parallel graph topologies, we allocate  $K$  orthogonal subcarriers. We explore configurations with  $K \in \{1, 2, 4, 8, 16\}$ . Each subcarrier  $k$  is assigned a bandwidth of  $B_k = 400$  kHz, separated by a guard band  $\Delta_f = 100$  kHz to prevent inter-carrier interference (e.g.,  $f_1 = 28.0000$  GHz,  $f_2 = 28.0005$  GHz, etc.). The nodes operate under a strict power constraint of  $P_{\text{tot}} = 0$  dBm, which must be dynamically allocated across the  $K$  active subcarriers.

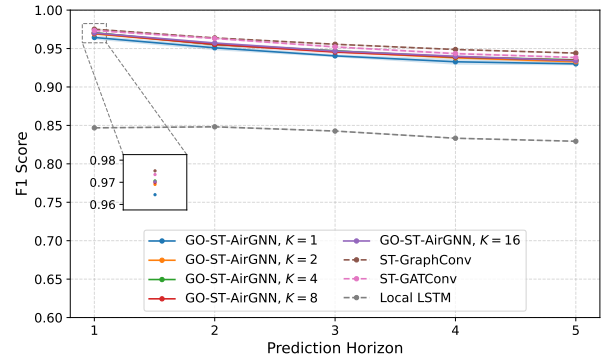
3) *Dataset Generation and Splitting:* We generate a training set  $\mathcal{T}_{\text{train}}$  and a test set  $\mathcal{T}_{\text{test}}$ , each comprising 1000 independent time-series realizations with  $N = 25$  nodes. For each realization, the IIoT nodes are randomly deployed in valid positions within the facility, ensuring spatial diversity. The two datasets include disjoint node positions to evaluate the inductive generalization capability of our framework to unseen topologies.

4) *Implementation and Hyperparameters:* The local transmission modules, i.e., the semantic encoder  $\Phi_i$  and the resource manager  $\Psi_i$ , are realized via multi-layer perceptrons (MLPs). For the receiver-side semantic decoder  $\chi_i$ , we employ a 2-layer long short term memory (LSTM) network with

<sup>2</sup>See: <https://bi-rex.it/en/>.



(a) Accuracy.



(b) F1 score.

Fig. 5: Performance evaluation of inductive generalization on unseen graph topologies.

64 hidden units. This recurrent structure allows the node to effectively integrate the temporal history of the spatially aggregated signals. The message embedding dimension is set to  $d = 64$ . To prioritize ultra-low latency inference, which is critical for the real-time IIoT control loop, we restrict the architecture to a *single* GNN aggregation layer for both the proposed method and the baselines. The model is trained end-to-end using the Adam optimizer. To ensure statistical reliability, all reported results represent the average of 10 independent trials with different random seeds.

5) *Baselines*: To validate the effectiveness of the proposed goal-oriented analog aggregation, we benchmark GO-ST-AirGNN against three distinct architectures:

- **Local LSTM**. This baseline operates in a purely non-cooperative manner. Each node attempts to predict blockages relying solely on the temporal history of its own local features  $\mathbf{x}_{i,t}$ , without exchanging information with neighbors. This serves as a performance *lower bound*, quantifying the fundamental gain yielded by spatial collaboration.
- **Spatio-temporal graph convolutional network (ST-GCN)**. This baseline combines standard spectral graph convolution with the temporal LSTM decoder. It aggregates neighbor features treating all connected neighbors with equal importance. It represents a topology-agnostic digital approach.
- **Spatio-temporal graph attention network (ST-GAT)**. This architecture employs digital attention mechanisms to assign importance weights to different neighbors. We include it to compare our proposed *physical* weighting strategy against a standard *digital* weighting approach, where neighbor relevance is computed computationally rather than via channel selection.

*Remark on Digital Baselines.* It is crucial to interpret ST-GCN and ST-GAT as *empirical reasoning upper bounds*, because they are granted perfect, instantaneous digital data exchange to assess the maximum possible prediction accuracy achievable with perfect information sharing. However, they ignore the physical reality of the wireless channel. In a real-world deployment, these digital methods would be subject to orthogonal access constraints, incurring in latency penalties, different from the proposed GO-ST-AirGNN.

## B. Inductive Generalization

A key characteristic of graph-based learning is *inductive generalization*, i.e., the ability of a model trained on specific graph structures in  $\mathcal{T}_{\text{train}}$  to generalize to unseen topologies in  $\mathcal{T}_{\text{test}}$ . In the context of IIoT, this property is crucial, as the deployment of active nodes in a facility often change dynamically. In Fig. 5, we present the quantitative results of our inductive generalization experiment in terms of accuracy and F1 score across prediction horizons ranging from 1 to 5 steps. A distinct performance gap is observed between the non-cooperative Local LSTM and all graph-based approaches. This confirms that blockage events in dynamic industrial environments cannot be reliably predicted solely from local history and spatial context from neighbors is essential to anticipate incoming blockages.

The proposed GO-ST-AirGNN demonstrates competitive performance, compared to the state-of-the-art graph baselines with ideal digital communication, while accounting for channel characteristics of actual physical environments. We remark that these state-of-the-art baselines overlook practical impairments of the wireless channel and assume sufficiently large communication resources [Section V-A]; hence, being considered as theoretical upper bounds only for reference. This indicates that our model is inherently able to deal with the superposition of analog signals for feature aggregation. Both accuracy and F1 scores of all approaches show a gradual decline as the prediction horizon  $\tau$  increases from 1 to 5, corresponding to a more challenging prediction problem. GO-ST-AirGNN maintains satisfactory performance, and increasing the number of parallel frequencies  $K$  yields improved results, which corroborate our theoretical findings that more communication resources provide stronger expressive power [Section V-B]. These results demonstrate that the proposed GO-ST-AirGNN possesses a strong generalization capacity, while featuring significantly higher spectral efficiency.

*Remark on Practical Expressivity and Latency.* It is important to emphasize that while the theoretical proof of expressivity (Proposition 2) relies on the availability of sufficient orthogonal resources to match representational capabilities of digital GNNs, empirical results shown in Fig. 5 suggest that such strict orthogonality is not a prerequisite for effective task performance. GO-ST-AirGNN maintains high accuracy even when  $K$  is small, exhibiting remarkable robustness to the

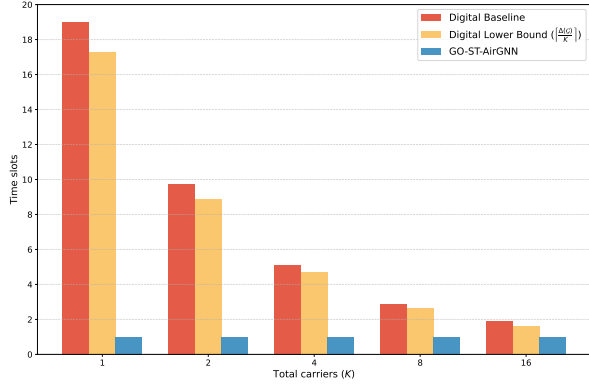


Fig. 6: Comparison of communication latency.

number of subcarriers. This indicates that the architecture is inherently capable of processing non-orthogonal signal superpositions effectively. As shown in Fig. 6, digital counterparts operating in this low- $K$  regime suffer from severe latency penalties. The figure illustrates this by plotting the actual digital performance alongside its theoretical lower bound. The latency of digital approaches scales linearly with the neighborhood size ( $T_{\text{dig}} \propto \frac{\Delta(\mathcal{G})}{K}$ ). In contrast, GO-ST-AirGNN scales effectively, achieving constant use of a single time slot independent of network density. Consequently, the proposed over-the-air aggregation proves to be more suitable for dense, resource-constrained networks than standard digital approaches.

### C. Robustness to Domain Shift

Next, we evaluate the robustness of GO-ST-AirGNN to domain shifts, including different mobile blockers than those seen during training. We test the trained model on an additional dataset  $\mathcal{T}'_{\text{test}}$ , which features a mobile robot with a significantly different physical shape compared to the one in the training set. To simulate a realistic rapid deployment scenario, we assume access to a scarce adaptation dataset  $\mathcal{T}'_{\text{adapt}}$  comprising only 10 graph time series, in sharp contrast to the 1000 sequences available in  $\mathcal{T}_{\text{train}}$  and  $\mathcal{T}'_{\text{test}}$ . For clarity, we present the performance of GO-ST-AirGNN with  $K = \{4, 16\}$  and digital graph baselines. Fig. 7 reports the accuracy across varying prediction horizons under three operational modes:

- 1) **Zero-Shot.** The model trained on the original environment is applied directly to the new domain without any updates.
- 2) **Transfer Learning.** The semantic encoder modules ( $\Phi$  and  $\Psi$ ) are *frozen*. Only the receiver-side semantic decoder  $\chi$  is fine-tuned on the new data. This represents a lightweight adaptation strategy where the communication protocol remains fixed.
- 3) **Full Adaptation.** The entire end-to-end pipeline ( $\Phi, \Psi, \chi$ ) is fine-tuned on the new domain.

First, we observe that the *Zero-Shot* performance naturally degrades due to the mismatch in blockage signatures between the training and test environments. However, the *Transfer Learning* strategy of the proposed GO-ST-AirGNN proves exceptionally effective. By fine-tuning only the local semantic decoder  $\chi_i$  on the scarce adaptation dataset  $\mathcal{T}'_{\text{adapt}}$  (while keeping the transmission policy  $\Phi_i, \Psi_i$  frozen), the system

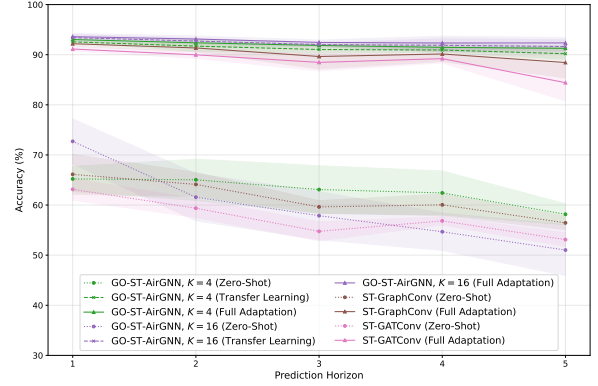


Fig. 7: Adaptation to domain shift.

recovers nearly the entire performance gap, i.e., the accuracy of the transfer learning approach converges to that of the *Full Adaptation*, where the entire pipeline is retrained. This implies a fundamental decoupling in the learned architecture: the *encoder* learns a robust and general communication strategy that remains valid across different environments, while the *decoder* handles the specific interpretation of the local blockage dynamics. It allows for rapid, low-complexity adaptation at the edge without requiring network-wide re-calibration. Second, as illustrated in Fig. 7, GO-ST-AirGNN with either transfer learning or full adaption outperforms ST-GCN and ST-GAT with full adaption, demonstrating that the proposed framework delivers stronger robustness and adaptability compared to digital graph baselines. These results confirm that our goal-oriented analog approach achieves competitive or even better performance than digital baselines under domain shifts. Moreover, these results further confirm that GO-ST-AirGNN provides an effective strategy to reduce communication cost while exhibiting competitive performance.

### D. Analysis of Goal-Oriented Power Allocation

In this section, we interpret how GO-ST-AirGNN utilizes the spectral domain according to its goal-oriented resource management policy. To isolate the specific contribution of the goal-oriented resource management module  $\Psi(\cdot)$ , we conduct an ablation study in Fig. 8. For conciseness, the results depicted in this figure are averaged over all considered prediction horizons  $\tau \in \{1, \dots, 5\}$ . We compare the *Learned* power allocation policy against two heuristic baselines: (i) *Uniform*, where the power budget  $P_{\text{tot}}$  is distributed equally across all  $K$  subcarriers; and (ii) *Random*, where the power allocation is sampled from a uniform distribution subject to the budget constraint. As illustrated in Fig. 8(a), the *Learned* strategy consistently yields the highest prediction accuracy across all configurations of  $K$ , confirming that learning the underlying topologies of communication graphs aids the aggregation process. In Fig. 8(b), we analyze the sensitivity of the system to the maximum transmission power budget  $P_{\text{tot}}$ , varying the constraint from  $-20$  dBm to  $10$  dBm. The accuracy curves exhibit a steeper improvement in the low-power regime followed by a plateau starting at approximately  $-5$  dBm, indicating that the system can operate in an energy-efficient regime without compromising prediction reliability.

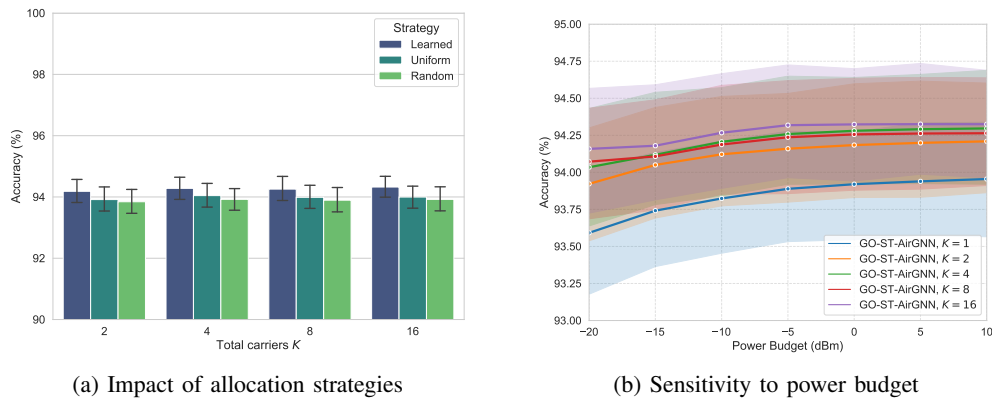


Fig. 8: Ablation study on goal-oriented power management.

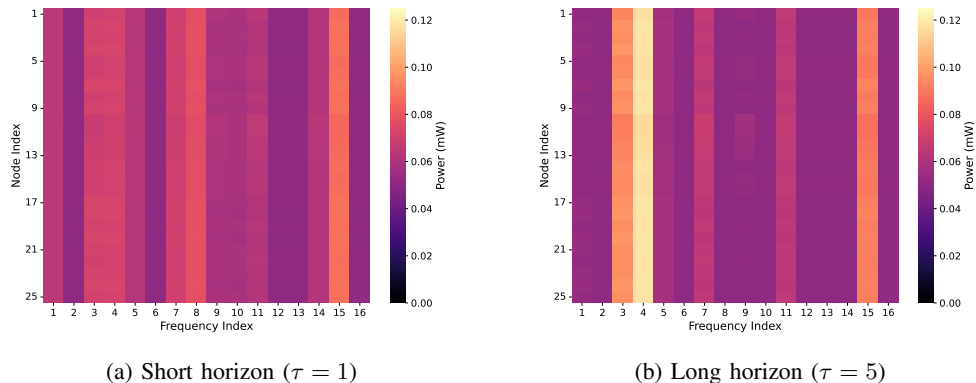


Fig. 9: Visualization of learned goal-oriented power allocation strategies, suggesting task-adaptive topology shaping.

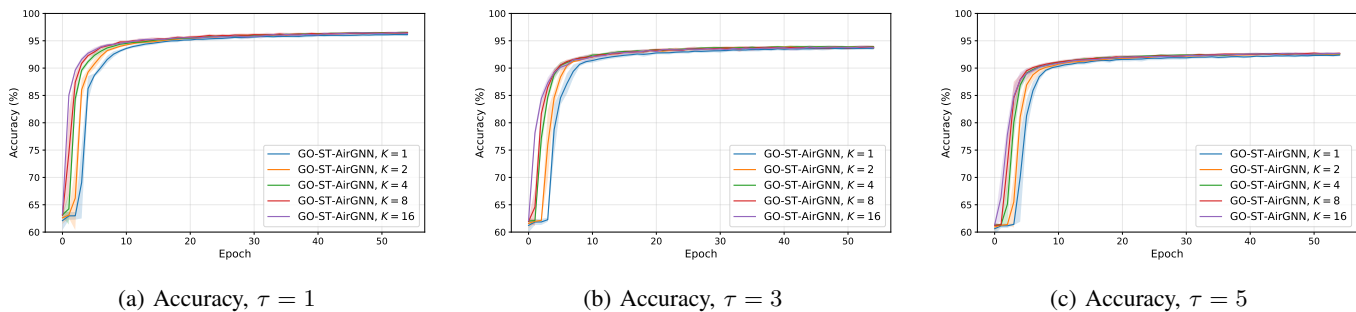


Fig. 10: Training convergence analysis.

To understand how the goal-oriented policy  $\Psi(\cdot)$  optimizes the graph topology, we visualize the power allocation matrices in Fig. 9. Considering GO-ST-AirGNN operating with  $K = 16$ , the heatmaps depict examples of transmitting power levels allocated by  $N = 25$  nodes across the available subcarriers for  $\tau = 1$  and  $\tau = 5$ . A common feature across both scenarios is that the allocation is generally non-sparse; nodes tend to utilize the entire spectral budget rather than selecting a single subcarrier, suggesting that GO-ST-AirGNN leverages the diversity of the  $K$  parallel graphs to build a robust ensemble, reinforcing local connectivity. Comparing Fig. 9a ( $\tau = 1$ ) and Fig. 9b ( $\tau = 5$ ) reveals a clear shift in strategy based on the difficulty of the prediction task. For the former case, the power distribution is relatively balanced. Since the blockage event is imminent, strong local

correlations are sufficient. In the latter case, instead, as the prediction horizon extends, the causal relationship between current features and future blockages becomes more complex and often requires capturing spatially distant dynamics (e.g., an approaching robot detected by a far neighbor). To address this, the policy shifts to allocate more power to a specific subcarrier, visible as bright vertical yellow bands in Fig. 9b, facilitating reliable longer-range information exchanges that are critical for anticipating future system states. This behavior empirically demonstrates the goal-oriented nature of the architecture: the physical graph topology is not static, but is dynamically reshaped to match the specific spatio-temporal requirements of the downstream prediction task. Therefore, the communication strategy (i.e., message passing operations) is learned contingent on the learning goal.

### E. Training Convergence Analysis

While the considered CTDE paradigm relies on offline training, evaluating the convergence trends of GO-ST-AirGNN provides critical insights into its learning efficiency. Fig. 10 shows training convergence trends. Notably, increasing the number of subcarriers  $K$  from 2 to 16 significantly enhances convergence speed across all considered scenarios ( $\tau = 1, 3, 5$ ). This acceleration can be attributed to the increased spectral diversity and resource granularity provided by a larger  $K$ . These additional degrees of freedom effectively smooth the optimization landscape, allowing the system to identify optimal topological configurations more rapidly. Overall, all variants exhibit highly stable training behavior, consistently reaching convergence plateaus within just 15-20 epochs, validating the method's robustness.

## VIII. CONCLUSION

In this paper, we introduced GO-ST-AirGNN, a goal-oriented communication framework that integrates AirComp with spatio-temporal graph learning to address the critical challenge of LOS blockage prediction in dense IIoT environments. Unlike digital methods, GO-ST-AirGNN utilizes the wireless channel as an analog processor and exploits wireless signal superposition to conduct feature aggregation effectively in non-orthogonal regimes. Our theoretical and empirical analysis yielded three key insights:

- The proposed architecture offers a decisive scalability advantage, achieving constant communication cost independent of node density, whereas digital baselines scale linearly with the neighborhood size of the communication graph.
- The expressivity of the analog aggregation via AirComp is comparable to its digital counterparts, providing a universal approximation in terms of expressive capacity.
- High-fidelity simulations demonstrated that the learned policies of GO-ST-AirGNN exhibit strong inductive generalization to unseen network topologies and can adapt to domain shifts via lightweight transfer learning.

It is worth noting that GO-ST-AirGNN achieves competitive performance even with very limited number of carriers, effectively unlocking scalability gains.

Looking forward, these findings open a promising avenue for establishing low-latency and spectral-efficient networked systems, where AirComp leverages superposition of analog signals for feature aggregation and goal-oriented communications align resource management with decision-making strategies for downstream tasks. Additionally, future research will explore the application of our framework to distinct sensing tasks that impose unique constraints on graph topology shaping, alongside an extension to distributed training schemes.

## APPENDIX

*Proof of Proposition 1.* The proof relies on the analysis of radio resource constraints in both schemes.

1) *GO-ST-AirGNN:* In the proposed scheme, the aggregation target for node  $i$  over the  $k$ -th resource is the weighted sum  $\tilde{\mathbf{y}}_{i,k} = \sum_{j \in \mathcal{D}_i} \mathbf{h}_{j,i,k} \tilde{\mathbf{x}}_{j,k}$ . This operation is mapped directly to the superposition property of the wireless channel, where every node  $j \in \mathcal{N}$  transmits its feature vector  $\mathbf{x}_j$  simultaneously over resource  $k$ . Since the channel naturally

performs the summation over-the-air, interference is treated as the aggregation operator rather than a collision. Consequently, all neighborhood aggregations for all  $i \in \mathcal{N}$  are completed in a single time slot. It follows that  $T_{\text{air}} = 1$ .

2) *Digital GNN:* In a digital scheme, node  $i$  must decode individual messages from every neighbor  $u \in \mathcal{D}_i$  to compute the aggregation digitally. This imposes a strict *orthogonality constraint*: signals from distinct neighbors  $u, v \in \mathcal{D}_i$  targeting the same receiver  $i$  must be orthogonal in time or frequency to avoid decoding failure. We formalize this resource allocation as a *graph coloring problem* [56]. Let  $\mathcal{G}_c = (\mathcal{N}, \mathcal{E}_c)$  be the *conflict graph* of the network. Two nodes  $u$  and  $v$  share an edge in the conflict graph  $\mathcal{E}_c$  if and only if they are distinct and share a common receiver (i.e., they are both neighbors of the same node  $i$ ), i.e.,

$$\mathcal{E}_c = \bigcup_{i \in \mathcal{N}} \{(u, v) \mid u, v \in \mathcal{D}_i, u \neq v\}, \quad (15)$$

where  $\bigcup(\cdot)$  is the union operator. The orthogonality constraint implies that for any receiver  $i$ , all its neighbors  $\mathcal{D}_i$  must be assigned distinct resources. Mathematically, the subgraph induced by  $\mathcal{D}_i$  in  $\mathcal{G}_c$  forms a *clique* of size  $|\mathcal{D}_i|$ , i.e., a graph where every node is connected to every other node. A fundamental property of graph coloring is that the minimum number of resources  $\rho(\mathcal{G}_c)$  needed to achieve orthogonal resource assignments for  $\mathcal{D}_i$  is lower-bounded by the size of the largest clique  $\omega(\mathcal{G}_c)$  in the graph, because all nodes in a clique are mutually adjacent and must therefore be assigned distinct resources. It follows that

$$\rho(\mathcal{G}_c) \geq \omega(\mathcal{G}_c) = \max_i |\mathcal{D}_i| = \Delta(\mathcal{G}). \quad (16)$$

Given a bandwidth budget of  $K$  parallel subcarriers per time slot, the number of time slots required is:

$$T_{\text{dig}} = \left\lceil \frac{\rho(\mathcal{G}_c)}{K} \right\rceil \geq \left\lceil \frac{\Delta(\mathcal{G})}{K} \right\rceil. \quad \square \quad (17)$$

### *Proof of Proposition 2.*

The proof relies on the capacity of GO-ST-AirGNN to orthogonalize communication links in the frequency domain at any time slot  $t$ . While  $K$  parallel channel realizations exist between any node pair  $(i, j)$ , we need only *one* active subcarrier to convey the message  $\mathcal{M}(\mathbf{u}_i, \mathbf{u}_j)$ . If  $K$  is large enough, we can assign distinct frequencies to distinct edges, preventing the channel from forcing an over-the-air aggregation and allowing the decoder to recover individual messages.

1) *Frequency Assignment:* As discussed in the proof of Proposition 1, this resource allocation problem can be framed as a graph coloring problem. If  $\mathcal{G}_c$  is conflict graph of the network and  $\rho(\mathcal{G}_c)$  is the minimum number of resources needed to satisfy the orthogonality constraint, it follows that  $K' = \rho(\mathcal{G}_c)$  is the number of subcarriers needed by a standard MPNN update rule to assign orthogonal frequencies to active links. Since  $K = K'$ , there exists an injective mapping  $\nu : \mathcal{E} \rightarrow \{1, \dots, K\}$  that assigns an interference-free subcarrier  $k^* = \nu(j, i)$  to every directed link  $(j, i)$ . This ensures that no two active transmissions in the network occupy the same frequency.

2) *Transmission Strategy:* Given phase synchronization, the effective channel is represented by its magnitude  $|\mathbf{h}_{j,i,k^*}|$ . To achieve deterministic message transfer, the system must invert these channel gains. First, the semantic encoder  $\Phi_j$  constructs

a unit-power message embedding  $\mathbf{m}_j$  carrying the semantic content:

$$[\mathbf{m}_j]_{k^*} = \mathcal{M}(\mathbf{u}_i, \mathbf{u}_j), \quad \text{with } |[\mathbf{m}_j]_{k^*}|^2 = 1. \quad (18)$$

Second, the resource management network  $\Psi_j$  allocates transmit power  $p_{j,k^*}$  to invert the channel gain:

$$p_{j,k^*} = \frac{P_{\text{rx}}}{|\mathbf{h}_{j,i,k^*}|}, \quad (19)$$

where  $P_{\text{rx}}$  is a target received signal power. This inversion is feasible provided the required power is within the budget, i.e.,  $p_{j,k^*} \leq P_{\text{tot}}$ .

3) *Analog Reception with Noise*: At receiver  $i$ , the signal on the unique assigned subcarrier  $k^*$  is the product of the channel gain, the transmit power scaling, and the message embedding. Due to the injectivity of  $\nu$ , there is no interference. The received signal is:

$$\begin{aligned} \tilde{\mathbf{y}}_{i,k^*} &= |\mathbf{h}_{j,i,k^*}| \cdot p_{j,k^*} \cdot [\mathbf{m}_j]_{k^*} + \mathbf{z}_{i,k^*} \\ &= |\mathbf{h}_{j,i,k^*}| \cdot \frac{P_{\text{rx}}}{|\mathbf{h}_{j,i,k^*}|} \cdot \mathcal{M}(\mathbf{u}_i, \mathbf{u}_j) + \mathbf{z}_{i,k^*} \\ &= P_{\text{rx}} \cdot \mathcal{M}(\mathbf{u}_i, \mathbf{u}_j) + \mathbf{z}_{i,k^*}, \end{aligned} \quad (20)$$

where  $\mathbf{z}_{i,k^*} \sim \mathcal{CN}(0, \sigma^2)$  is the thermal noise.

4) *Semantic Decoding*: The received vector  $\mathbf{y}_i$  now contains the separated messages  $\{\mathcal{M}(\mathbf{u}_i, \mathbf{u}_j)\}_{j \in \mathcal{N}_i}$  scaled by  $P_{\text{rx}}$ , plus noise. The semantic decoder  $\chi_i$ , acting as a universal function approximator, can be trained to: (a) Normalize the input entries by  $1/P_{\text{rx}}$  to recover the original message scale (while ignoring inactive subcarriers). (b) Apply the desired aggregation operator  $\oplus$  (e.g., max, mean) over the recovered messages. (c) Apply the update function  $\mathcal{U}$ .

Eq. 20 reveals that the over-the-air reconstruction is inherently stochastic due to thermal noise  $\mathbf{z}_{i,k^*}$ . However, the approximation becomes exact in the high-SNR regime. Specifically, if the power budget  $P_{\text{tot}}$  is sufficient such that  $\frac{P_{\text{tot}}}{\sigma^2} \rightarrow \infty$ , the effect of  $\mathbf{z}_{i,k^*}$  becomes negligible relative to the signal, and GO-ST-AirGNN converges to the deterministic MPNN behavior. Thus, the output  $\hat{\mathbf{y}}_{i,t+\tau}$  approximates the generic MPNN layer, proving the proposition.  $\square$

## REFERENCES

- [1] K. B. Letaief, W. Chen, Y. Shi, J. Zhang, and Y.-J. A. Zhang, "The roadmap to 6G: AI empowered wireless networks," *IEEE Communications Magazine*, vol. 57, no. 8, pp. 84–90, 2019.
- [2] E. C. Strinati, D. Belot, A. Falempin, and J.-B. Doré, "Toward 6G: From new hardware design to wireless semantic and goal-oriented communication paradigms," in *ESSCIRC 2021 - IEEE 47th European Solid State Circuits Conference (ESSCIRC)*, 2021, pp. 275–282.
- [3] W. Saad, M. Bennis, and M. Chen, "A vision of 6G wireless systems: Applications, trends, technologies, and open research problems," *IEEE network*, vol. 34, no. 3, pp. 134–142, 2019.
- [4] T.-Y. Tung, S. Kobus, J. P. Roig, and D. Gündüz, "Effective communications: A joint learning and communication framework for multi-agent reinforcement learning over noisy channels," *IEEE Journal on Selected Areas in Communications*, vol. 39, no. 8, pp. 2590–2603, 2021.
- [5] F. Pezone, S. Barbarossa, and P. Di Lorenzo, "Goal-oriented communication for edge learning based on the information bottleneck," in *ICASSP 2022-2022 IEEE International Conference on Acoustics, Speech and Signal Processing (ICASSP)*. IEEE, 2022, pp. 8832–8836.
- [6] D. Wen, P. Liu, G. Zhu, Y. Shi, J. Xu, Y. C. Eldar, and S. Cui, "Task-oriented sensing, computation, and communication integration for multi-device edge AI," *IEEE Transactions on Wireless Communications*, vol. 23, no. 3, pp. 2486–2502, 2023.
- [7] W.-Q. Ren, Y.-B. Qu, C. Dong, Y.-Q. Jing, H. Sun, Q.-H. Wu, and S. Guo, "A survey on collaborative DNN inference for edge intelligence," *Machine Intelligence Research*, vol. 20, no. 3, pp. 370–395, 2023.
- [8] W. Wu, P. Yang, W. Zhang, C. Zhou, and X. Shen, "Accuracy-guaranteed collaborative DNN inference in industrial IoT via deep reinforcement learning," *IEEE Transactions on Industrial Informatics*, vol. 17, no. 7, pp. 4988–4998, 2021.
- [9] N. Longhi, L. M. Amorosa, S. Cavallero, E. Buracchini, and R. Verdone, "5G architectures enabling remaining useful life estimation for industrial IoT: A holistic study," *IEEE Open Journal of the Communications Society*, vol. 6, pp. 1016–1029, 2025.
- [10] Y. E. Sagduyu, S. Ulukus, and A. Yener, "Age of information in deep learning-driven task-oriented communications," in *IEEE INFOCOM 2023 - IEEE Conference on Computer Communications Workshops (INFOCOM WKSHPS)*, 2023, pp. 1–6.
- [11] Z. Wang, Y. Zhao, Y. Zhou, Y. Shi, C. Jiang, and K. B. Letaief, "Over-the-air computation for 6G: Foundations, technologies, and applications," *IEEE Internet of Things Journal*, vol. 11, no. 14, pp. 24 634–24 658, 2024.
- [12] M. Frey, I. Bjelaković, and S. Stańczak, "Over-the-air computation for distributed machine learning and consensus in large wireless networks," in *Compressed Sensing in Information Processing*. Springer, 2022, pp. 401–434.
- [13] Z. Gao, F. Gama, and A. Ribeiro, "Wide and deep graph neural network with distributed online learning," *IEEE Transactions on Signal Processing*, vol. 70, pp. 3862–3877, 2022.
- [14] Y. Lu, Y. Li, R. Zhang, W. Chen, B. Ai, and D. Niyato, "Graph neural networks for wireless networks: Graph representation, architecture and evaluation," *IEEE Wireless Communications*, vol. 32, no. 1, pp. 150–156, 2025.
- [15] L. M. Amorosa, L. Spampinato, C. Buratti, and R. Verdone, "Goal-oriented uplink scheduling requests in wireless networks via graph neural networks," in *IEEE EUROCON 2025 - 21st International Conference on Smart Technologies*, 2025, pp. 1–6.
- [16] Z. Gao and D. Gündüz, "Graph neural networks over the air for decentralized tasks in wireless networks," *IEEE Transactions on Signal Processing*, vol. 73, pp. 721–737, 2025.
- [17] J. Zhang, W. Lu, C. Xing, N. Zhao, N. Al-Dhahir, G. K. Karagiannidis, and X. Yang, "Intelligent integrated sensing and communication: a survey," *Science China Information Sciences*, vol. 68, no. 3, p. 131301, 2025.
- [18] A. Shastri, N. Valecha, E. Bashirov, H. Tataria, M. Lentmaier, F. Tufvesson, M. Rossi, and P. Casari, "A review of millimeter wave device-based localization and device-free sensing technologies and applications," *IEEE Communications Surveys & Tutorials*, vol. 24, no. 3, pp. 1708–1749, 2022.
- [19] B. Zhou, X. Wang, Y. Shen, and P. Fan, "6-DoF location-and-pose estimation toward integrated visible light communication and sensing: Algorithm design and performance limits," *IEEE Transactions on Signal Processing*, vol. 72, pp. 2576–2593, 2024.
- [20] Y. Gao, Y. Ai, B. Tian, L. Chen, J. Wang, D. Cao, and F.-Y. Wang, "Parallel end-to-end autonomous mining: An IoT-oriented approach," *IEEE Internet of Things Journal*, vol. 7, no. 2, pp. 1011–1023, 2019.
- [21] S. Das, D. Sen, E. Viterbo, A. K. R. Chavva, D. Sharma, and A. Nigam, "Ambit-process-based spatial-wideband MIMO channel model for sub-THz urban microcellular communication," *IEEE Transactions on Wireless Communications*, vol. 23, no. 1, pp. 559–574, 2023.
- [22] Y. Chen, C. Han, Z. Yu, and G. Wang, "Channel measurement, characterization, and modeling for terahertz indoor communications above 200 GHz," *IEEE Transactions on Wireless Communications*, vol. 23, no. 6, pp. 6518–6532, 2023.
- [23] Y. Yang, S. Dang, M. Wen, B. Ai, and R. Q. Hu, "Blockage-aware robust beamforming in RIS-aided mobile millimeter wave MIMO systems," *IEEE Transactions on Wireless Communications*, 2024.

- [24] Y. Yang, F. Gao, X. Tao, G. Liu, and C. Pan, "Environment semantics aided wireless communications: A case study of mmWave beam prediction and blockage prediction," *IEEE journal on selected areas in communications*, vol. 41, no. 7, pp. 2025–2040, 2023.
- [25] P. Wang, K. Ma, Y. Bai, C. Sun, and Z. Wang, "Deep learning assisted mmWave beam prediction with flexible network architecture," *IEEE Transactions on Wireless Communications*, 2025.
- [26] A. Bonfante, L. G. Giordano, I. Macaluso, and N. Marchetti, "Performance of predictive indoor mmWave networks with dynamic blockers," *IEEE Transactions on Cognitive Communications and Networking*, vol. 8, no. 2, pp. 812–827, 2021.
- [27] S. Wu, M. Alrabeiah, C. Chakrabarti, and A. Alkhateeb, "Blockage prediction using wireless signatures: Deep learning enables real-world demonstration," *IEEE Open Journal of the Communications Society*, vol. 3, pp. 776–796, 2022.
- [28] S. Wu, C. Chakrabarti, and A. Alkhateeb, "LiDAR-aided mobile blockage prediction in real-world millimeter wave systems," in *2022 IEEE Wireless Communications and Networking Conference (WCNC)*. IEEE, 2022, pp. 2631–2636.
- [29] G. Charan, M. Alrabeiah, and A. Alkhateeb, "Vision-aided 6G wireless communications: Blockage prediction and proactive handoff," *IEEE Transactions on Vehicular Technology*, vol. 70, no. 10, pp. 10 193–10 208, 2021.
- [30] U. Demirhan and A. Alkhateeb, "Radar aided proactive blockage prediction in real-world millimeter wave systems," in *ICC 2022-IEEE International Conference on Communications*. IEEE, 2022, pp. 4547–4552.
- [31] M. Skocaj, T. Zugno, J. Blumenstein, and M. Boban, "Line of sight blockage prediction via spatio-temporal graph neural networks," in *2024 IEEE Globecom Workshops (GC Wkshps)*, 2024, pp. 1–6.
- [32] S. Jamshidiha, V. Pourahmadi, A. Mohammadi, and M. Bennis, "Power allocation using spatio-temporal graph neural networks and reinforcement learning," *Wireless Networks*, vol. 31, no. 2, pp. 1163–1176, 2025.
- [33] N. Mehregan and E. Robson, "GCN-based throughput-oriented handover management in dense 5G vehicular networks," in *2025 21st International Conference on Distributed Computing in Smart Systems and the Internet of Things (DCOSS-IoT)*. IEEE, 2025, pp. 895–902.
- [34] J. Jiang, Y. Li, Y. Ye, D. Feng, J. Zhang, W. Sutthiphpan, and D. Niyato, "Spatio-temporal GNN-based cell-free massive MIMO network with maximal benefit-cost ratio," *IEEE Transactions on Vehicular Technology*, 2025.
- [35] F. Corradini, F. Gerosa, M. Gori, C. Lucheroni, M. Piangerelli, and M. Zannotti, "A systematic literature review of spatio-temporal graph neural network models for time series forecasting and classification," *Neural Networks*, p. 108269, 2025.
- [36] G. Zhu, Y. Wang, and K. Huang, "Broadband analog aggregation for low-latency federated edge learning," *IEEE Transactions on Wireless Communications*, vol. 19, no. 1, pp. 491–506, 2020.
- [37] A. Şahin and R. Yang, "A survey on over-the-air computation," *IEEE Communications Surveys & Tutorials*, vol. 25, no. 3, pp. 1877–1908, 2023.
- [38] Y. Yang, Y. Wu, Y. Jiang, and Y. Shi, "One-bit byzantine-tolerant distributed learning via over-the-air computation," *IEEE Transactions on Wireless Communications*, vol. 23, no. 6, pp. 5441–5455, 2023.
- [39] Z. Wang, Y. Zhou, Y. Zou, Q. An, Y. Shi, and M. Bennis, "A graph neural network learning approach to optimize RIS-assisted federated learning," *IEEE Transactions on Wireless Communications*, vol. 22, no. 9, pp. 6092–6106, 2023.
- [40] Y. Yang, Z. Zhang, Y. Tian, R. Jin, and C. Huang, "Implementing graph neural networks over wireless networks via over-the-air computing: A joint communication and computation framework," *IEEE Wireless Communications*, vol. 30, no. 3, pp. 62–69, 2023.
- [41] M. Lee, G. Yu, and H. Dai, "Privacy-preserving decentralized inference with graph neural networks in wireless networks," *IEEE Transactions on Wireless Communications*, vol. 23, no. 1, pp. 543–558, 2023.
- [42] C. Feng, K. Zheng, Y. Wang, K. Huang, and Q. Chen, "Goal-oriented wireless communication resource allocation for cyber-physical systems," *IEEE Transactions on Wireless Communications*, 2024.
- [43] T. M. Getu, G. Kaddoum, and M. Bennis, "Making sense of meaning: A survey on metrics for semantic and goal-oriented communication," *IEEE Access*, vol. 11, pp. 45 456–45 492, 2023.
- [44] H. Zhang, H. Wang, Y. Li, K. Long, and A. Nallanathan, "DRL-driven dynamic resource allocation for task-oriented semantic communication," *IEEE Transactions on Communications*, vol. 71, no. 7, pp. 3992–4004, 2023.
- [45] W. Wu, Y. Yang, Y. Deng, and A. H. Aghvami, "Goal-oriented semantic communications for robotic waypoint transmission: The value and age of information approach," *IEEE Transactions on Wireless Communications*, 2024.
- [46] Y. Cheng, D. Niyato, H. Du, J. Kang, Z. Xiong, C. Miao, and D. I. Kim, "Resource allocation and common message selection for task-oriented semantic information transmission with RSMA," *IEEE Transactions on Wireless Communications*, vol. 23, no. 6, pp. 5557–5570, 2023.
- [47] Z. Gao, Y. Shao, D. Gündüz, and A. Prorok, "Decentralized channel management in WLANs with graph neural networks," in *ICC 2024 - IEEE International Conference on Communications*, 2023, pp. 3072–3077.
- [48] L. M. Amorosa, M. Skocaj, R. Verdone, and D. Gündüz, "Multi-agent reinforcement learning for power control in wireless networks via adaptive graphs," in *ICC 2024 - IEEE International Conference on Communications*, 2024, pp. 2968–2973.
- [49] L. M. Amorosa, Z. Gao, T. Chahoud, R. Verdone, and D. Gündüz, "Decentralized GNN-based power allocation with varying network density," in *2025 IEEE International Conference on Machine Learning for Communication and Networking (ICMLCN)*, 2025, pp. 1–6.
- [50] A. Mahmood, M. I. Ashraf, M. Gidlund, J. Torsner, and J. Sachs, "Time synchronization in 5G wireless edge: Requirements and solutions for critical-MTC," *IEEE Communications Magazine*, vol. 57, no. 12, pp. 45–51, 2019.
- [51] O. Abari, H. Rahul, D. Katabi, and M. Pant, "AirShare: Distributed coherent transmission made seamless," in *2015 IEEE Conference on Computer Communications (INFOCOM)*. IEEE, 2015, pp. 1742–1750.
- [52] A. Şahin and R. Yang, "Over-the-air computation over balanced numerals," in *2022 IEEE Globecom Workshops (GC Wkshps)*. IEEE, 2022, pp. 347–352.
- [53] F. Wang, J. Xu, V. K. Lau, and S. Cui, "Amplify-and-forward relaying for hierarchical over-the-air computation," *IEEE Transactions on Wireless Communications*, vol. 21, no. 12, pp. 10 529–10 543, 2022.
- [54] L. Chen, N. Zhao, Y. Chen, F. R. Yu, and G. Wei, "Over-the-air computation for IoT networks: Computing multiple functions with antenna arrays," *IEEE Internet of Things journal*, vol. 5, no. 6, pp. 5296–5306, 2018.
- [55] J. Hoydis, F. A. Aoudia, S. Cammerer, M. Nimier-David, N. Binder, G. Marcus, and A. Keller, "Sionna RT: Differentiable ray tracing for radio propagation modeling," in *2023 IEEE Globecom Workshops (GC Wkshps)*, 2023, pp. 317–321.
- [56] P. M. Pardalos, T. Mavridou, and J. Xue, "The graph coloring problem: A bibliographic survey," in *Handbook of Combinatorial Optimization: Volume1–3*. Springer, 1998, pp. 1077–1141.